Uncertainty quantification for linear and weakly non-linear supersonic boundary-layer instability

By O. Marxen, G. Iaccarino AND E. S. G. Shaqfeh

1. Motivation and objectives

Laminar-turbulent transition in compressible, high-speed boundary layers is currently not well understood. The transition location on the surface of a vehicle can therefore not accurately be predicted. This is particularly true for transition on surfaces with a localized two-dimensional unevenness, such as a roughness element (Balakumar 2003; Marxen *et al.* 2009). Cases with geometrical changes are relevant for a number of applications, including the heat-shield of vehicles (re-)entering a planetary atmosphere and the inlet to scram jet combustors for hypersonic cruise vehicles. Transition is undesirable on the heat shield due to an associated increase in temperature. It is desirable for scram jets to ensure proper mixing within the combustor.

In all theses applications an accurate prediction of the transition location is advantageous for the vehicle design. Presently, many transition prediction methods rely on a deterministic description in which a fixed transition location is computed. Examples are correlation-based methods and the e^N-method (Malik 1989). Typical N-factors at transition lie in the range of $5 - 10$ (see examples in Malik 2003).

Recently, Crouch (2008) proposed to account for growth modifiers, such as two–dimensional steps, by adding a ΔN to the N-factor. Herein we consider the linear evolution of an explicitly forced perturbation in a flat-plate boundary layer, with a to-dimensional roughness acting as a growth modifier. In addition to a deterministic description, we take a probabilistic approach to account for uncertainties in the height of the roughness. This is motivated by the observation that accidental roughness created by deposition or impact can only be measured approximately.

Numerical simulations with explicitly forced perturbations, the so-called controlled transition, have been criticized as not being representative of situations where such forcing is absent, the so-called natural transition. While the former approach has often been adopted in fundamental investigation of transition mechanisms at low levels of free-stream turbulence, the latter situation is regarded as more relevant in engineering applications. A commonly accepted way to treat the natural transition has not yet emerged.

Let us assume that the essential difference between the two situations lies in the fact that the disturbance spectrum remains unspecified for the natural transition. Under this assumption, stochastic simulations, in which a number of deterministic simulations with explicitly forced perturbations are carried out, offer an attractive method to handle the uncertainty with respect to the disturbance spectrum. As a first step, we consider the secondary instability (Herbert 1988; Eissler & Bestek 1996), provided that we have only a statistical description of the amplitude of the primary perturbation.

The objective of this report is twofold. First, physical insight into the non-linear amplification of perturbations with fixed frequency will be gained. In contrast to the work by Eissler & Bestek (1996), these perturbations evolve in a supersonic boundary-layer with two-dimensional roughness. Second, a method will be introduced and applied that is able

to quantify the uncertainty in disturbance amplification. This uncertainty is associated with the availability of only limited information regarding the disturbance amplitude.

2. Mathematical model and numerical method for flow simulations

Numerical simulations are based on an algorithm described in Nagarajan *et al.* (2003). Solutions to the compressible Navier-Stokes equations are obtained, applying sixth-order compact finite-differences together with third-order explicit Runge-Kutta time stepping. The numerical discretization is constructed on a structured, curvilinear grid using staggered variables. No explicit shock-capturing scheme is present as occurring shocks are sufficiently weak so that they can be treated by applying a high-order compact numerical filter. The fluid is assumed to be a calorically perfect gas, and the viscosity is computed from Sutherland's law. Details of the setup can be found in Marxen *et al.* (2009). In contrast to that reference, here we also consider the case of secondary amplification of disturbances.

The height of the roughness is on the order of, but typically smaller than, the boundary-layer thickness of the smooth flow. Disturbances of fixed frequency and fixed spanwise wave number, are triggered via blowing and suction at the wall close to the inflow boundary (in two dimensions: $(\rho v)_w = A_v^{2-D} \times f(x) \times g(t)$ with $f, g \in [0, 1]$ so that the magnitude of $(\rho v)_w$ is determined by A_v^{2-D}).

Two different cases are studied. First, a linear case is considered in which the evolution of the single forced two-dimensional disturbance is independent of its amplitude. Second, a weakly non-linear case of secondary instability is investigated. In addition to a finite-amplitude primary two-dimensional wave, a pair of small-amplitude oblique waves, with half the frequency of the primary wave and a non-zero spanwise wave number, are forced (with a fixed phase difference between the two). Due to subharmonic resonance, the oblique waves can experience stronger amplification than in the absence of the two-dimensional wave, if the amplitude of this two-dimensional wave is sufficiently large.

2.1. *Grid resolution and verifcation*

For the two-dimensional simulations presented here we used 800 equidistant grid points in the streamwise dimension x for a domain extending from $R_x = 401$ to $R_x = 1736$ with $R_x = \sqrt{x \cdot Re_\infty}$, whereas in the wall-normal direction y, 201 grid points were used on a stretched grid for a domain height $y_{max} = 1.575$ (at the inflow: $y_{max}/\delta^* = 34.32$). Marxen *et al.* (2009) verified this resolution to be sufficient.

For three-dimensional simulations, the disturbance with non-zero spanwise wave number still behaves linearly. Only a low resolution of 10 spanwise grid points per wave length was necessary to accurately capture the disturbance evolution. This has been verified by repeating the simulation with twice the number of spanwise grid points, which gives results that are indistinguishable from the lower resolved ones to plotting accuracy (Fig. 1). In the streamwise and wall-normal direction, the same discretization as for the two-dimensional cases has been applied.

3. Uncertainty quantification

3.1. *Description of the method*

Both, the linear and the non-linear cases depend parametrically on a (case-dependent) random variable s, respectively. This parameter s is assumed to lie within a certain inter-

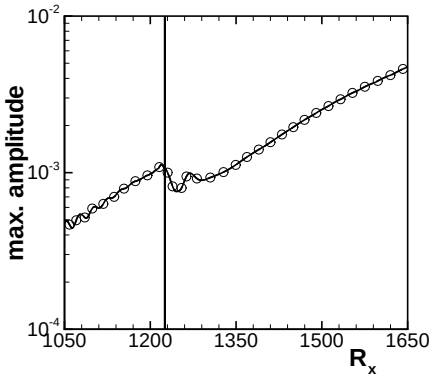

FIGURE 1. Amplitude $\hat{u}^{max}_{(1/2,\pm1)}$ for $h_R = 0.125$ with $A_v^{2-D} = 0.035$. Results with a spanwise resolution of 10 grid points (line) and 20 grid points (symbols). For a description of the case see section 5.2.

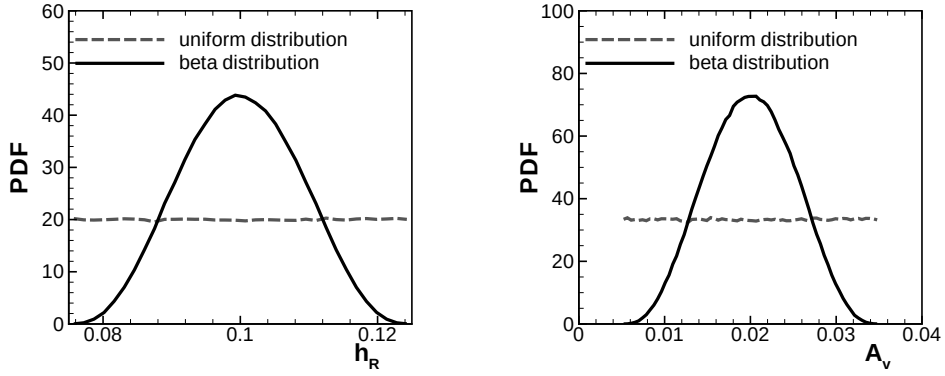

FIGURE 2. Histograms for assumed PDFs for the Monte Carlo method. Left: linear case (for a description of the case, see section 5.1). Right: non-linear case (see section 5.2).

val: $s \in [s_{min}, s_{max}]$. It is distributed either uniformly or according to a beta distribution. Based on a random number $q \in [0, 1]$, s can be obtained from a linear transformation:

$$s(q) = q \times (s_{max} - s_{min}) + s_{min}\,. \tag{3.1}$$

For the beta distribution, the probability density function (PDF) for q is defined as follows, here with a choice $(\alpha, \beta) = (4, 4)$:

$$q \sim \text{beta}(\alpha, \beta), \text{with PDF}(q; \alpha, \beta) = \frac{q^{\alpha-1}(1-q)^{\beta-1}}{\int_0^1 u^{\alpha-1}(1-u)^{\beta-1}\mathrm{d}u}\,. \tag{3.2}$$

Histograms for the resulting PDFs are depicted in Fig. 2 in terms of assumed uncertainty in the height of the roughness and the amplitude.

We apply non-intrusive stochastic collocation. In this technique, a value for s, i.e., s^m, is chosen and then a simulation is performed. Once the simulation is completed, the quantity of interest p is computed based on the simulation result (a definition for p is given in section 6). We perform a sequence of M simulations, giving M deterministic

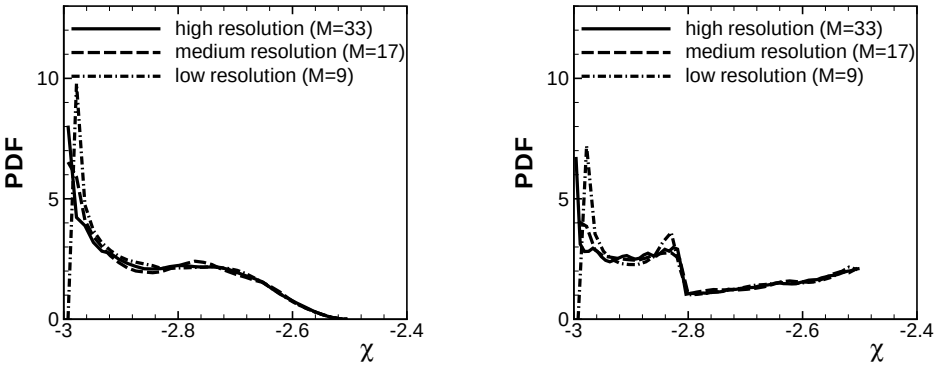

FIGURE 3. PDFs for χ at $R_x = 1550$ for the non-linear case for three different resolutions using 34 bins. Left: $s = A_v^{2-D}$ chosen according to a beta distribution. Right: $s = A_v^{2-D}$ chosen according to a uniform distribution.

values p^m. A nested rule is applied to chose the collocation points for $s^m{=}s(q^m)$ on the abscissae. We employ the Clenshaw-Curtis rule (Trefethen 2008):

$$q^m = (1 - \cos(\pi(m-1)/(M-1)))/2 \text{ with } m = 1 \dots M\,. \tag{3.3}$$

In a final step, the obtained values p^m are used to compute a PDF for the quantity p. This is achieved by means of Monte Carlo sampling as a post-processing procedure. For this sampling standard random generators are used, delivering a random number $q \in [0, 1]$. The corresponding s is computed from Eq. (3.1). The response $p(s)$ is approximately built as an interpolant of the collocation points using a Lagrange polynomial:

$$p(s) \approx p_C^M = \Sigma_{m=1}^M p^m L_m(s) \text{ with } L_m(s) = \Pi_{k=1,k\neq m}^M (s - s^k)/(s^m - s^k)\,. \tag{3.4}$$

Here we have computed $1,000,000$ results $p(s)$ based on as many samples s. All the $p(s)$ are sorted into bins in the range $min(p^{m=1\dots M})$ to $max(p^{m=1\dots M})$ to form a PDF histogram.

3.2. *Verification*

Varying the number of abscissas M gives an estimate of the influence of this parameter on the resulting PDFs. Here, we have computed these PDFs considering only results for half or a quarter of all M available results p^m in addition to using the full resolution. We found that for the linear case, $M{=}9$ abscissa points are sufficient, and results for $M = 17$ did not visibly change the resulting PDF for both initial PDFs assumed here. For the non-linear case, differences are visible as depicted in Fig. 3, but nevertheless are regarded as acceptable.

The number of Monte Carlo samples, here $1,000,000$ as stated above, was also found to be sufficient. Increasing the number of abscissa points M can be very expensive, because every new point requires a new simulation. In contrast, increasing the number of Monte Carlo samples is computationally much less expensive.

4. Mean flow

Only a brief overview of the mean flow ($Re_\infty = 10^5$, $Pr_\infty = 0.71$, $Ma_\infty = 4.8$, $\gamma_\infty = 1.4$, Sutherland's law with $\tilde{T}_S/\tilde{T}_\infty = 1.993$, adiabatic wall) is given here; more

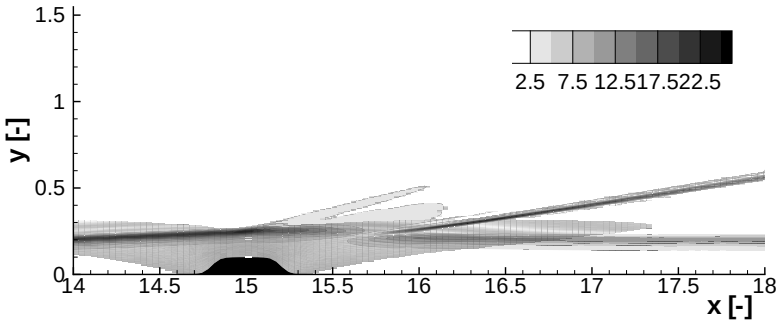

FIGURE 4. Contours of the absolute wall-normal density gradient $|\partial\rho/\partial y|$ for roughness $h_R = 0.1$.

details can be found in Marxen *et al.* (2009). A representation of the mean flow field is given in Fig. 4 by means of a numerical Schlieren image. Boundary-layer separation occurs both upstream and downstream of the roughness. For $h_R = 0.1$, the ratio between the boundary-layer thickness δ_{99}, based on $\tilde{u}/\tilde{u}_\infty$=0.99 for the flat-plate at the center location of the roughness ($x = 15$), and the roughness height is $h_R/\delta_{99} \approx 0.55$.

The roughness element causes a compression followed by an expansion, which again is followed by a compression. The latter causes a weak oblique shock downstream of the roughness element, well visible in the region $x > 15.8$, $y > 0.2$, in Fig. 4. The expansion downstream of the roughness leads to an acceleration of the flow in the free stream. This acceleration causes the streamlines to turn toward the wall after they have been deflected away from the wall by the roughness. Finally, downstream of the roughness the shock causes the stream lines to become roughly wall parallel, again.

The localized roughness element leads to boundary-layer separation both in the upstream and downstream regions. On top of the roughness, a thin attached boundary layer forms. For $h_R = 0.1$, the length of the separation bubbles upstream and downstream differ roughly by a factor of two: its length is approximately $13h_R$ upstream of the roughness and $6h_R$ downstream of it. This observation is consistent with reports of Balakumar (2003) for a boundary layer at Mach 3.5.

5. Deterministic disturbance evolution

The evolution of disturbances in the flow field with a two-dimensional roughness is described only for selected deterministic simulations (isothermal wall with $T_w = T_{w,adiabatic}$). Results for the streamwise velocity are Fourier transformed in time t and span z with a fundamental circular frequency $F = 2\pi\tilde{f}\left(\tilde{\mu}/(\tilde{\rho}\tilde{u}^2)\right)_\infty = 10^{-4}$ and a fundamental spanwise wave number $\gamma = 2\pi/\lambda_z = 10.4$. Then, the maximum over y is computed to yield amplitudes $\hat{u}^{max}_{(h,k)}$. The notation (h, k) is used to refer to a disturbance with a frequency $h \times F$ and a spanwise wave number $k \times \gamma$.

In the linear case, the modification in disturbance evolution caused by the roughness is quantified based on the change in N-factor, defined as:

$$\Delta N = \ln\left((A(h_R))/(A(\text{flat plate}))\right) \text{ with } A = \hat{u}^{max}_{(1,0)}\,. \tag{5.1}$$

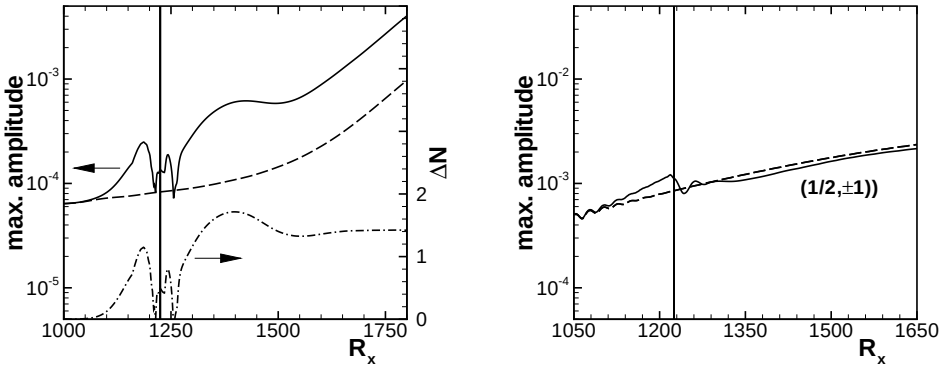

FIGURE 5. Amplitude $\hat{u}^{max}_{(h,k)}$ for $h_R = 0.125$ (——) and a flat plate (– –). The vertical lines mark the center location of the roughness. Left: $(h,k) = (1,0)$ with $A_v^{2-D} = 4.17\times10^{-4}$, together with the respective ΔN (–·–). Right: $(h,k) = (1/2,\pm1)$ with $A_v^{3-D} = 1.00\times10^{-4}$.

5.1. *Primary instability*

Fig. 5 (left) compares the two-dimensional disturbance evolution, mode $(1,0)$, for the streamwise velocity component between the case with height $h_R = 0.125$ and a flat plate ($R_x = \sqrt{Re_\infty \times x}$). The roughness acts as a local growth modifier, causing the disturbance amplitude downstream to be significantly larger compared with that of the flat plate. Far downstream, the same amplification as for the flat-plate case is recovered, and ΔN approaches a constant value. The effect of the roughness is less pronounced for lower frequencies. For an oblique wave with half the frequency of the previously considered two-dimensional wave, the roughness has a slightly damping effect (Fig. 5, right). Downstream of the roughness, the same amplification as for the flat-plate case is recovered.

Marxen *et al.* (2009) investigated the linear disturbance evolution in the boundary-layer with two-dimensional roughness in detail. Their findings are summarized in the following.

The separating boundary layer boosts the amplification of both first(inflectional)- and second(acoustic)-type instability mechanisms as a result of more convectively unstable boundary-layer profiles. This boost is concentrated at lower frequencies as the frequency-range of the second-type instability shifts toward lower values owing to an increase in boundary-layer thickness. The overall maximum amplification rate is found within the region of the adverse-pressure gradient upstream of the roughness, and the instability in front of the roughness is independent of the (downstream) length of the roughness. The lower the roughness height the weaker the effect on the instability, both in terms of spatial expansion but also with regard to the maximum amplification rate.

Downstream of the roughness, an additional disturbance is generated and interacts with the one coming from upstream. As a result, the disturbance signal behind the roughness exhibits a beating: constructive (and destructive) interference occurs. The additional disturbance is stable, but possesses a phase velocity similar to the unstable mode in the vicinity of the roughness. Far downstream, the amplification rate of a flat plate for the same distance from the leading edge is recovered.

Along the roughness, the disturbance is always found to be strongly damped. Because of this damping, for disturbances at low frequencies the net effect is zero despite an increased

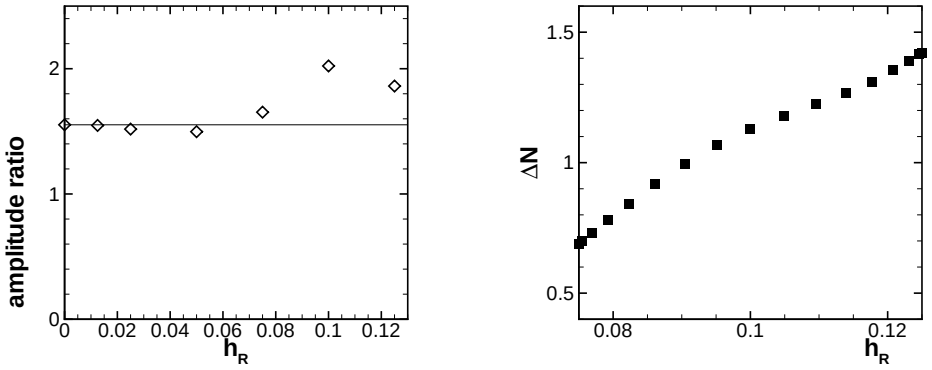

FIGURE 6. Left: density ratio $\hat{\rho}_1^{max}(R_x = 1680)/\hat{s}_1^{max}(R_x = 1200)$ versus height of the roughness element with $l_R = 0.4$, adiabatic wall boundary condition. The horizontal lines mark the ratio observed for the flat plate $h_R \equiv 0$. Right: response curve for the linear two-dimensional case, isothermal wall boundary condition, i.e., ΔN as a function of roughness height h_R.

amplification upstream of the roughness. At high frequencies (second-type instability even without roughness), the net effect is even strongly negative, i.e., the far downstream amplitude is significantly smaller than for a flat plate. For disturbances within a certain frequency range, the presence of the roughness changes the instability mechanism from first to second type in the vicinity of the roughness. For these disturbances, a gain in amplitude over the flat-plate case is observed. A frequency in this range, namely $F = 1\times10^{-4}$, is considered as the primary disturbance frequency for subsequent investigations of non-linear disturbance evolution.

5.1.1. *Influence of the roughness height*

The effect of roughness height is considered in more detail for the most dangerous frequency. For a roughness larger than $h_R = 0.0125$, the ratio of the amplitude upstream and downstream of the roughness becomes a strong function of the roughness height (Fig. 6, left), which suggests that the effect of roughness can not be captured by a linear model. This is particularly true for a range of roughness heights that are considered in stochastic simulations. Deterministic simulation results for this range, using an isothermal wall boundary condition, are depicted in Fig. 6 (right). Here, the disturbance amplitude far downstream increases monotonically with roughness height.

5.2. *Secondary instability*

In the non-linear case, the modification in disturbance evolution caused by the finite-amplitude two-dimensional wave is quantified. To reinforce the importance of absolute disturbance amplitude for transition, we define a transition parameter χ as follows:

$$\chi = \log\left(\hat{u}^{max}_{(1/2,\pm1)}\right). \tag{5.2}$$

If χ reaches values larger than a certain threshold χ_c, transition may be imminent (the exact threshold for transition remains to be determined). This may make $x_T = x|_{\chi=\chi_c}$ a simple criterion for the transition location x_T. In Fig. 7 (left), differences between the non-linear case with two-dimensional roughness and the linear case for a flat plate is not seen simply in the vicinity of the roughness. Instead, the growth of the oblique waves, which is enhanced by subharmonic resonance, continues to be larger because of the large-

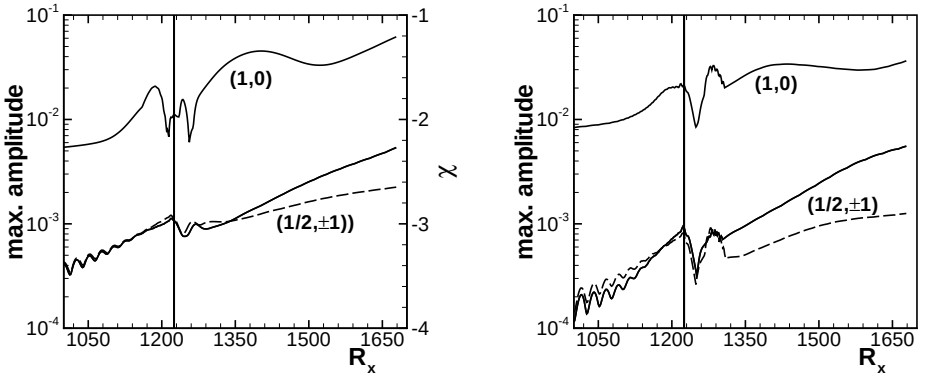

FIGURE 7. Amplitudes $\hat{a}^{max}_{(h,k)}$ for $h_R = 0.125$ with $A_v^{2-D} = 0.035$ (——) and $A_v^{2-D} = 0.0$ (– –). Quantities $a = u$ (left) and $a = \rho$ (right).

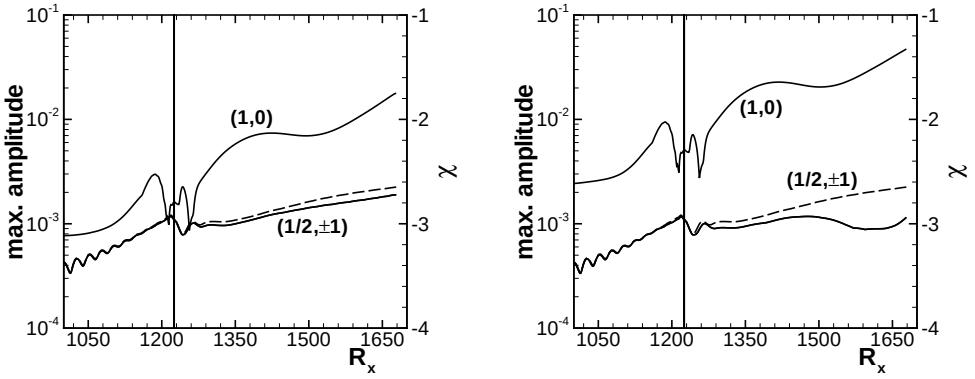

FIGURE 8. Same as Fig. 7 (left), but for $A_v^{2-D} = 0.005$ (left) and $A_v^{2-D} = 0.0156$ (right).

amplitude two-dimensional waves. For a similar setup, Eissler & Bestek (1996) did not observe a significant subharmonic resonance because they had smaller two-dimensional amplitudes in their simulations.

5.2.1. *Influence of the amplitude of the primary wave*

In order to investigate the effect of the amplitude of the primary wave, a range of values for this amplitudes has been considered. The result depicted in Fig. 7 corresponds to the largest amplitude considered, in which case a significant increase of amplification could be observed. For the smallest amplitude considered (Fig. 8, left), the primary disturbance had a small damping effect. This effect was even more pronounced for an intermediate amplitude (Fig. 8, right).

All the results for different two-dimensional primary amplitudes are compiled in Fig. 9, where the value of χ downstream of the roughness is given as a function of primary amplitude. This graph represents the response curve used for the stochastic approach.

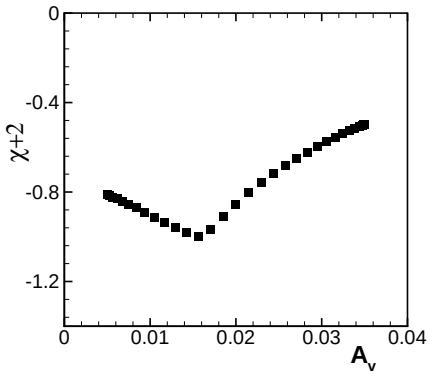

FIGURE 9. Response curve for the non-linear case, i.e., χ at $R_x = 1550$ for a roughness height $h_R = 0.125$ as a function of primary amplitude.

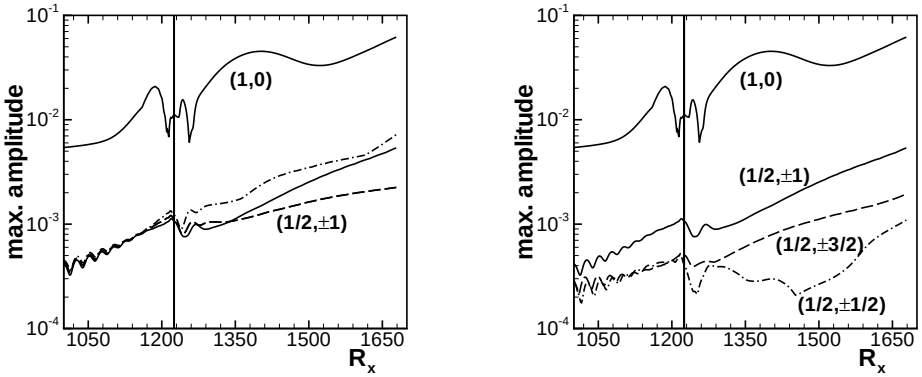

FIGURE 10. Left: same as Fig. 7 (left), but results for two different values of the phase difference at the location of their respective disturbance strip $\Delta\Psi = 0$ (——) and $\Delta\Psi = \pi/2$ (– · –). The linear evolution is given for reference (– –). Right: same as Fig. 7 (left), but results for three different spanwise wave length as given by the respective labels in the diagram.

5.2.2. *Influence of the phase difference between the primary and the secondary wave*

The way the primary and the secondary waves become resonant is dependent not only on the amplitude of the primary wave but also on the respective phase differences as it can be seen in Fig. 10 (left). A difference between the amplification rates should not occur far downstream of the roughness once the two waves have gone into resonance. However, this state has not been reached yet for the streamwise length of the domain considered here owing to moderate secondary amplification rates.

5.2.3. *Influence of the spanwise wave number*

The spanwise wave number considered previously, $\gamma = 10.4$, lies in the range of the most amplified wave numbers for a frequency $F = 0.5 \times 10^{-4}$ for the present case according to linear stability theory (see figure 6 in Marxen *et al.* 2009). This is confirmed in Fig. 10 (right) in the region upstream of the roughness, where effects of secondary instability are still small. While the secondary amplification downstream of the roughness is much stronger for a disturbance with a smaller spanwise wave length (the case with

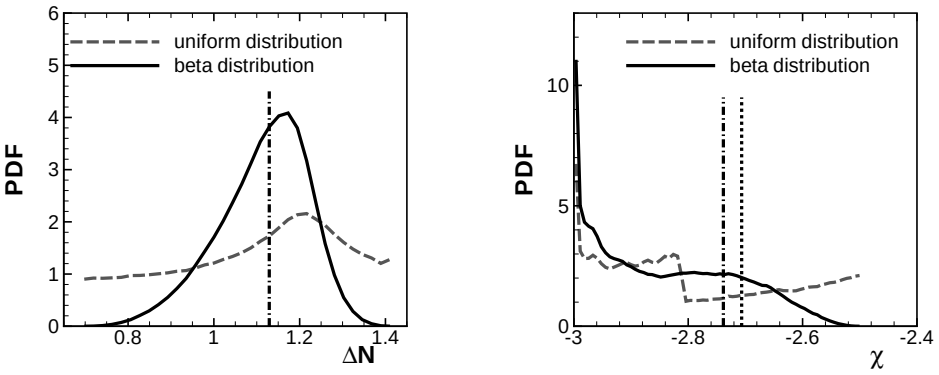

FIGURE 11. Left: PDFs for ΔN at $R_x = 1750$ for the linear case using 34 bins. The vertical line (– · –) marks the deterministic value for $h_R = 0.1$. Right: PDFs for χ at $R_x = 1550$ for the non-linear case using 68 bins. The vertical lines mark the value for linear disturbance evolution, $A_v^{2-D} = 0.0$, for a flat plate (– · –) and for $h_R = 0.125$ (· · · · ·).

(h, k)=$(1/2, \pm 1/2)$), the maximum amplitude is still reached for the spanwise wavenumber $k = 1$.

6. Stochastic disturbance evolution

The stochastic results discussed in the following are based on the simulation results described in section 5. They may be interpreted as resulting from a sophisticated way of post-processing of the simulation data, because our probabilistic approach is non-intrusive. A prerequisite, however, is a precise choice of collocation points for the simulations, that is a certain set of random parameters s. These lead to the distribution of abscissas in Fig. 6 (right) and Fig. 9, respectively.

6.1. *Linear case*

For the linear case the height of the roughness is taken as the random parameter $s = h_R$, and extrema in Eq. (3.1) are chosen as $s_{min} = 0.075$ and $s_{max} = 0.125$. The quantity of interest is the change in N-factor caused by the roughness, Eq. (5.1), sufficiently far downstream of the roughness $p = \Delta N|_{R_x=1750}$, and we have chosen M=17.

The resulting PDFs are presented in Fig. 11 (left) for a uniform distribution of roughness heights and a β-distribution centered around $h_R = 0.1$. In both cases, the PDFs have a local maximum at a value ΔN close to the deterministic result for $h_R = 0.1$. For a uniform distribution, this is a direct result of the inflection point of the response $\Delta N(h_R)$ (Fig. 6, right) at approximately $h_R = 0.105 \ldots 0.11$, $\Delta N = 1.2$.

6.2. *Non-linear case*

For the non-linear case, the forcing amplitude of the two-dimensional wave is the random parameter $s = A_v^{2-D}$, with $s_{min} = 0.005$ and $s_{max} = 0.035$. The quantity of interest is the parameter χ, Eq. (5.2), again downstream of the roughness $p = \chi|_{R_x=1550}$ (M=33).

The PDFs for the non-linear case (Fig. 11, right) show two interesting features. First, the non-linear effects can lead to a damping. This causes a significant probability that the amplitude of the oblique wave is smaller than in the linear case. Second, the right-hand flank of the PDF is even qualitatively different for the two considered amplitude

distributions. This suggests that great care has to be taken in choosing a distribution in order to lead to an accurate prediction of transition for a given case.

Note that because the solution is linear in the disturbance amplitude of the oblique wave, the position of the PDF relative to the origin is, in fact, arbitrary.

7. Conclusion

The evolution of disturbances in a Mach 4.8 flat-plate boundary layer with a two-dimensional roughness element has been investigated. Deterministic simulations show that the two-dimensional roughness acts as an amplifier for convective disturbances, and the resulting increased disturbance amplitude can enhance a secondary instability. The dependence of the secondary instability for subharmonic resonance on several parameters has been discussed. These parameters included the amplitude of the primary wave, the phase difference between the primary and the secondary wave, and the spanwise wave number of the secondary wave. We found a local maximum in the probability density function for a certain increase in (linear) amplitude even for uniformly distributed roughness heights. As one possible first step toward a probabilistic description of transition, a stochastic approach has been applied to quantify the probability for an increased or decreased amplification.

8. Future work

Regarding the primary (linear) instability, the generation mechanism of the stable and an amplitude boost of the unstable mode in the presence of a two-dimensional roughness has been observed here, and this mechanism seems to be active in the rear of the roughness. However, an elucidation of the details of this mechanism certainly warrants further investigations.

An extension of the presented study of the secondary instability should include the case of fundamental resonance. Eissler & Bestek (1996) concluded that this scenario is more important than subharmonic resonance for the present setup on a flat plate, and it should be verified if the same still holds for the flow with a two-dimensional roughness. Furthermore, the domain should be extended further downstream to investigate lead transitional stages and breakdown to turbulence. However, this will require a significantly increased spanwise resolution.

In order to render the presented probabilistic approach to transition prediction more useful, a receptivity model is still required that provides the PDF for the amplitude of the primary wave. In an extension, additional random parameters such as the phase difference between the primary and the secondary wave and the spanwise wave number of the secondary wave should be included in the stochastic approach. This may be computationally very expensive and suggests the use of modern uncertainty quantification techniques in order to make this transition prediction feasible.

Acknowledgments

Financial support from the National Aeronautics and Space Administration (NASA) under award No. NNX07AC29A is gratefully acknowledged. We are grateful to S. Lele, Stanford University, for providing the finite-difference code.

REFERENCES

Balakumar, P. 2003 Transition in a supersonic boundary-layer due to roughness and acoustic disturbances. *AIAA Paper 2003–3589* .

Crouch, J. D. 2008 Modeling transition physics for laminar flow control. *AIAA Paper 2008–3832* .

Eissler, W. & Bestek, H. 1996 Spatial numerical simulations of linear and weakly nonlinear wave instabilities in supersonic boundary layers. *Theor. Comp. Fluid Dyn.* **8** (3), 219–235.

Herbert, T. 1988 Secondary instability of boundary layers. *Annu. Rev. Fluid Mech.* **20**, 487–526.

Malik, M. R. 1989 Prediction and control of transition in supersonic and hypersonic boundary layers. *AIAA J.* **27** (11), 1487–1493.

Malik, M. R. 2003 Hypersonic flight transition data analysis using parabolized stability equations with chemistry effects. *J. Spacecraft Rockets* **40** (3), 332–344.

Marxen, O., Iaccarino, G. & Shaqfeh, E. 2009 Disturbance evolution in a Mach 4.8 boundary layer with two-dimensional roughness-induced separation and shock. *JFM, accepted for publication* .

Nagarajan, S., Lele, S. K. & Ferziger, J. H. 2003 A robust high-order method for large eddy simulation. *J. Comput. Phys.* **191**, 392–419.

Trefethen, L. N. 2008 Is Gauss quadrature better than Clenshaw–Curtis? *SIAM Review* **50** (1), 67–87.